SCIENTIFIC REPORTS

OPEN

SUBJECT AREAS:
NONLINEAR PHENOMENA
VENTRICULAR TACHYCARDIA

Received
13 February 2014

Accepted
10 April 2014

Published
29 April 2014

Correspondence and requests for materials should be addressed to H.Z. (hongzhang@zju.edu.cn)

* These authors contributed equally to this work.

Unpinning of rotating spiral waves in cardiac tissues by circularly polarized electric fields

Xia Feng[1]*, Xiang Gao[1]*, De-Bei Pan[1], Bing-Wei Li[2] & Hong Zhang[1]

[1]Zhejiang Institute of Modern Physics and Department of Physics, Zhejiang University, Hangzhou 310027, China, [2]Department of Physics, Hangzhou Normal University, Hangzhou 310036, China.

Spiral waves anchored to obstacles in cardiac tissues may cause lethal arrhythmia. To unpin these anchored spirals, comparing to high-voltage side-effect traditional therapies, wave emission from heterogeneities (WEH) induced by the uniform electric field (UEF) has provided a low-voltage alternative. Here we provide a new approach using WEH induced by the circularly polarized electric field (CPEF), which has higher success rate and larger application scope than UEF, even with a lower voltage. And we also study the distribution of the membrane potential near an obstacle induced by CPEF to analyze its mechanism of unpinning. We hope this promising approach may provide a better alternative to terminate arrhythmia.

Spirals, also known as rotors[1] or vortices[2], occur in various excitable systems, including chemical media[3–5], aggregations of Dictyostelium discoideum amoebae[6], and cardiac tissues[7]. In hearts, spirals and subsequent turbulences may cause lethal arrhythmia[8–12]. Better than traditional therapies[13], a new approach using wave emission from heterogeneities (WEH) or far-field stimulation provides a promising alternative to terminate arrhythmia[14–17]. This approach is based on the fact that, by the application of an external electric field to a whole piece of tissue, de-polarizations and hyper-polarizations (so-called Weidmann zones[18]) could be induced near obstacles (conductivity heterogeneities). These obstacles correspond to blood vessels, ischemic regions, and smaller-scale discontinuities. If the electric strength exceeds some threshold, obstacles can act as virtual electrodes or second sources[19–25].

The life-saving motivation to terminate arrhythmia has sparked many discussions about the mechanism of WEH[26–32]. However, previous works focus on WEH in response to the uniform electric field (UEF), which is realized by applying DC pulses onto field electrodes[14–17]. Recently, the circularly polarized electric field (CPEF) has shown its unique ability to control spirals and turbulences[33,34], and has been verified in the Belousov-Zhabotinsky reaction by applying two ACs onto two pairs of field electrodes perpendicular to each other[35].

In this paper, we study the mechanism of WEH induced by CPEF, and find that its ability to unpin anchored spirals, which is an important step in terminating arrhythmia, has advantages over UEF, such as lower voltage, higher success rate and larger application scope. Therefore, as a lower-voltage higher-efficiency approach, CPEF is more applicable in terminating arrhythmia.

In the following, without loss of generality, we use a counter-clockwise rotating CPEF to unpin anchored spirals, which can be expressed as $\mathbf{E} = (E_x, E_y)$, where $E_x = E_0\cos(\omega_e t + \phi_e)$, $E_y = E_0\cos(\omega_e t + \phi_e + 3\pi/2)$ and E_0, ω_e, ϕ_e are its strength, angular frequency and initial phase relative to x axis. In mono-domain models, the general effect of an external electric field on an obstacle can be expressed as an additional no-flux boundary condition[26,29]: $\mathbf{n}\cdot\nabla(V + \mathbf{E}\cdot\mathbf{r}) = 0$, where $\mathbf{n}$ is the normal vector to the obstacle boundary, V is the membrane potential, $\mathbf{E}$ is the external electric field, and $\mathbf{r}$ is a point on the boundary. Therefore, in the presence of a circular obstacle (radius R) influenced by CPEF, the boundary condition can be described in the polar coordinate (ρ, θ) as

$$\partial_\rho V(\rho,\theta)\big|_{\rho=R} + E_0\cos(\theta - \omega_e t - \phi_e) = 0. \quad (1)$$

Our numerical analysis is based on the evolution equations, which describe the membrane potential V across the cellular membrane, along with a number of gating variables, collectively denoted as $\mathbf{y}$, characterizing the conductance of various ionic channels. Symbolically, the system can be expressed as

$$\partial_t V = -I_{ion}(V,\mathbf{y})/C + D\nabla^2 V$$
$$\partial_t \mathbf{y} = \boldsymbol{F}(\mathbf{y},V), \quad (2)$$

where functions I_{ion} and $\boldsymbol{F}$ are determined by different ionic currents in different models, C is the membrane capacitance, and D is the diffusion current coefficient. To demonstrate the results found in this paper are robust and essentially independent of precise ionic currents, we use both Luo-Rudy model[36] and Barkley model[37].

Based on equation (1), to describe the distribution of the membrane potential induced by CPEF near a circular obstacle, we apply CPEF at a weak strength in a two-dimensional quiescent medium. As shown in Fig. 1a (Luo-Rudy model) and 1c (Barkley model), the mechanism of WEH in response to CPEF rests on the induced de-polarization (red region) and hyper-polarization (blue region) near the obstacle. In both Luo-Rudy model and Barkley model, comparing to the dipole-like patterns induced by UEF[28,14–17] (Fig. 1b and 1d), the patterns induced by CPEF have two novel characters: one is that, they rotate synchronously with the rotating CPEF; the other is that, their patterns are similar as Chinese "ancient Taijitu". Depending on attaching to the obstacle or not, we divide both de-polarization and hyper-polarization into "Head" and "Tail" (Fig. 1a).

The stably-rotating and fantastically-shaped de-polarization and hyper-polarization elucidated above can be used to unpin anchored spirals if the CPEF's strength E_0 exceeds a certain value and angular frequency ω_e is tuned to a proper value. In cardiac tissues, anchored spirals may have clockwise or counter-clockwise rotating directions. Therefore, to get a more comprehensive understanding about unpinning by CPEF, we discuss these two types of rotating directions separately.

Firstly, we numerically simulate a clockwise rotating anchored spiral at the angular frequency ω_s and discuss its unpinning mechanism by CPEF. In Luo-Rudy model as shown in Fig. 2a, at t = 0, ϕ_e is the initial phase of CPEF relative to x axis, ϕ_s is the initial phase of the anchored spiral front relative to x axis. In cardiac tissues, ϕ_e is always given at a certain value, while ϕ_s would be arbitrary. But in order to keep wave patterns simple and get a convenient structure analysis by numerical simulations, we choose ϕ_e is arbitrary but restrict ϕ_s to zero. Furthermore, we can define the initial phase difference between ϕ_e and ϕ_s as $\Delta\phi = \phi_e - \phi_s$, to simply demonstrate the initial configuration of CPEF and the anchored spiral. Hence, the configuration at $t = 0$ in Fig. 2a can be defined as a given $\Delta\phi$. Then at $t = 20$ ms, a new wave **N** has been nucleated and begins to collide and merge with the anchored spiral **S**. Later at t = 40 ms, the colliding parts have detached from the obstacle, and form a new free spiral **S'**. Although there is another new wave **N'** nucleated by CPEF, its evolvement does not affect the final result. So after applying CPEF for a period in which an anchored spiral rotates one round ($2\pi/\omega_s$), there will be only **S'** left. And after ceasing CPEF for another period of $2\pi/\omega_s$, at $t = 105$ ms, **S'** does not re-pin to the obstacle but still keeps rotating freely. This is viewed as a "successful unpinning"[30].

Additionally, the unpinning procedure above is much clearer in Barkley model, as shown in Fig. 2b. At the start, the configuration of CPEF and the anchored spiral **S** is introduced by a given $\Delta\phi$. Then, at $t = 1.0$ when the phase of CPEF is $1.0\omega_e + \phi_e$, a new wave **N** has been nucleated by the de-polarization. The one end of **N**, corresponding to the "Head" of de-polarization, is going to collide with **S**. Later at $t =$

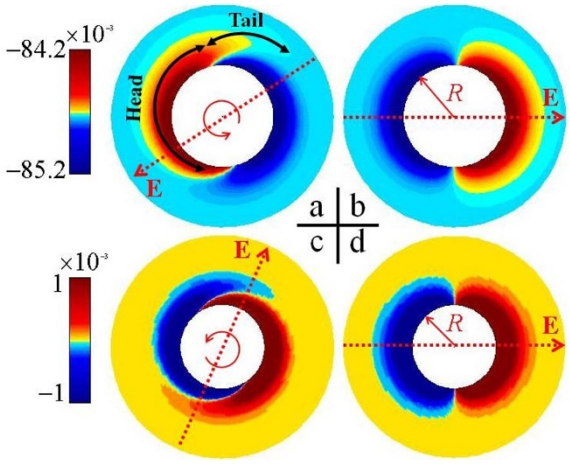

Figure 1 | Distribution of the membrane potential induced by CPEF and UEF. (a), CPEF in Luo-Rudy model, $E_0 = 0.05$ V/cm, $\omega_e = 0.2$ rad/ms. (b), UEF in Luo-Rudy model, $E_0 = 0.05$ V/cm. (c), CPEF in Barkley model, $E_0 = 0.05$, $\omega_e = 4$. (d), UEF in Barkley model, $E_0 = 0.05$. In this and following numerical simulations of Luo-Rudy model, the obstacle size $R = 0.32$ cm, and the excitability is set as same as in Ref. 38. In this and following numerical simulations of Barkley model, the obstacle size $R = 3$, and unless otherwise specified, the excitability is set as $a = 0.8$, $b = 0.06$. The obstacles are all applied additional no-flux boundary conditions as equation (1) shows. The red dotted arrows represent the directions of electric field. The red curved arrows mean CPEFs rotate counter-clockwise. The red and blue regions around obstacles demonstrate de-polarizations and hyper-polarizations, respectively. The two black double-headed arrows indicate how we divide the "Head" and "Tail". The patterns in (b) and (d) which we get from simulations are the same as in Fig. 1a of Ref. 28.

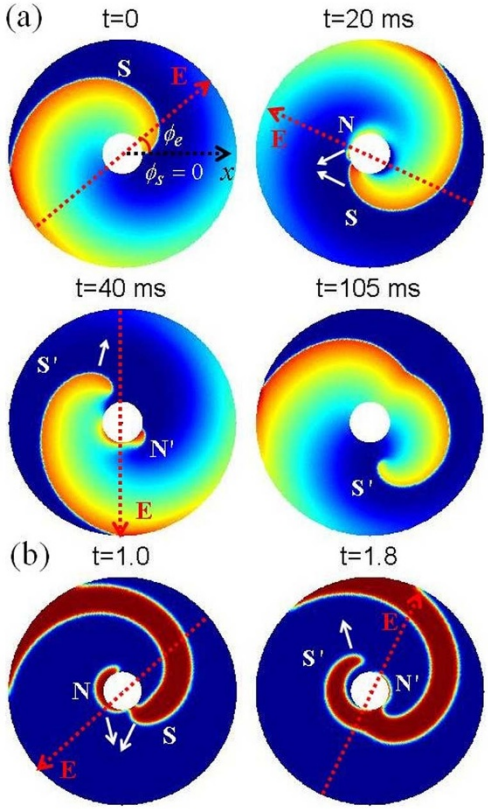

Figure 2 | Unpinning the clockwise rotating anchored spiral by CPEF. (a), In Luo-Rudy model, the angular frequency of spiral $\omega_s = 0.136$ rad/ms. The CPEF's strength $E_0 = 0.7$ V/cm and angular frequency $\omega_e = 0.1$ rad/ms. CPEF is applied from $t = 0$ to $t = 46.2$ ms. ϕ_e is the initial phase of CPEF relative to x axis, and ϕ_s is the initial phase of the anchored spiral front relative to x axis and set as zero. (b), In Barkley model, the angular frequency of spiral $\omega_s = 1.024$. The CPEF's strength $E_0 = 1.8$ and angular frequency $\omega_e = 3.686$. CPEF is applied from $t = 0$ to $t = 6$. **N** and **N'** represent different new waves nucleated by CPEF in different time. **S** and **S'** represent the initial anchord spiral and the new free spiral, respectively. White arrows are the propagation directions of waves.

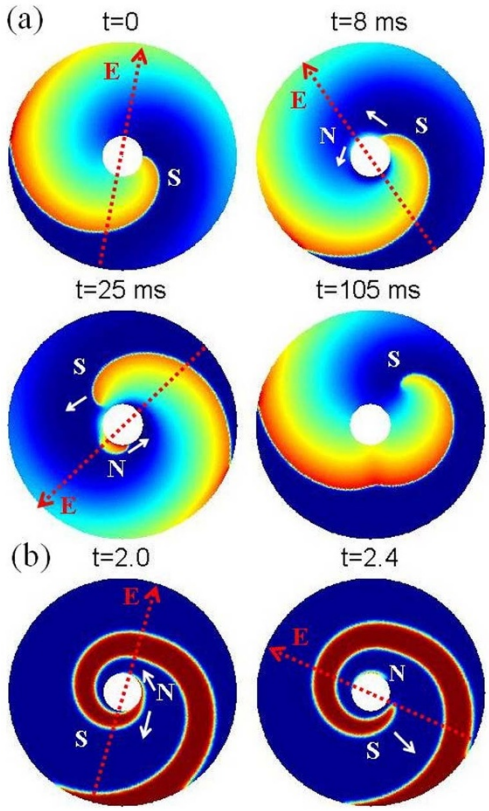

Figure 3 | Unpinning the counter-clockwise rotating anchored spiral by CPEF. (a), In Luo-Rudy model, the angular frequency of spiral $\omega_s = 0.136$ rad/ms. The CPEF's strength $E_0 = 0.7$ V/cm and angular frequency $\omega_e = 0.1$ rad/ms. CPEF is applied from $t = 0$ to $t = 46.2$ ms. (b), In Barkley model, the angular frequency of spiral $\omega_s = 1.024$. The CPEF's strength $E_0 = 1.8$ and angular frequency $\omega_e = 3.686$. CPEF is applied from $t = 0$ to $t = 6$.

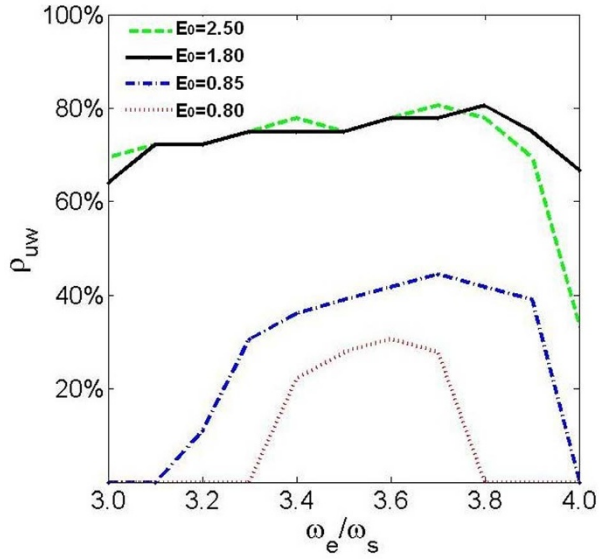

Figure 4 | The relations between ρ_{uw} and ω_e/ω_s in Barkley model. Different lines represent ρ_{uw} plotted against ω_e/ω_s under different E_0. We choose interval [3.0, 4.0] for instance to reflect the existence of the optimal ω_e/ω_s. Since the range centered around $\omega_e/\omega_s = 3.6$ has a relative large ρ_{uw} even under a weak electric strength (e.g. $E_0 = 0.8$, red dotted line), we adopt this ratio as the optimal ω_e/ω_s in following numerical simulations of Barkley model.

1.8, the colliding parts merge with each other. And the other end of **N**, corresponding to the "Tail" of de-polarization, has detached from the obstacle, because its propagation along the boundary of obstacle is inhibited by both the "Head" of hyper-polarization and the refractory tail of **S**. Thereby, **N** and **S** form a new unpinned spiral **S'**. Because of the continuing CPEF, another new wave **N'** has been nucleated by CPEF, but **N'** has no effect to the final result. Finally, **S'** can be viewed as a successfully unpinned spiral. Therefore, we can recognize such $\Delta\phi$ can lead to successful unpinning, and call it the proper $\Delta\phi$.

In the next, we discuss the other mechanism about unpinning a counter-clockwise rotating anchored spiral by CPEF with a proper $\Delta\phi$. In Luo-Rudy model (Fig. 3a), at the start of applying CPEF ($t = 0$), an anchored spiral **S** is counter-clockwise rotating around the obstacle. Then at $t = 8$ ms, a new wave **N** is nucleated by CPEF. Later at $t = 25$ ms, **S** is unpinned from the obstacle. Finally, at $t = 105$ ms, **S** rotates freely, which satisfy the requisite of successful unpinning.

The clearer process can be seen in Barkley model (Fig. 3b). Similarly at the start, the configuration of CPEF and the anchored spiral is introduced by a proper $\Delta\phi$. Then at $t = 2.0$, a new wave **N** is nucleated due to the de-polarization induced by CPEF. Later at $t = 2.4$, the anchored spiral **S** gradually falls into the "Head" of hyper-polarization induced by CPEF, which is at the opposite obstacle boundary of **N**. Because of the inhibition caused by the "Head" of hyper-polarization, **S** is unpinned. Furthermore, because of the inhibition caused by the "Tail" of hyper-polarization, **S** is driven further away from the obstacle. Although **N** is still rotating along the obstacle, it makes no effect to the final result and **S** will evolve to a successfully unpinned spiral.

To summarize, we get two types of unpinning mechanisms by CPEF: for a given CPEF and excitability, with the proper $\Delta\phi$, the rotating de-polarization and hyper-polarization induced by CPEF can lead to successful unpinning, corresponding to Figs. 2 and 3 respectively.

Therefore, we can consider $\Delta\phi$ is an important factor for successful unpinning. We define the whole range of $\Delta\phi$ which can lead to successful unpinning as the unpinning window $\{\Delta\phi\}_{\text{unpin}}$. Since $\Delta\phi$ is in the interval of $[0, 2\pi)$, $\{\Delta\phi\}_{\text{unpin}}$ can be normalized by 2π as

$$\rho_{\text{uw}} = \frac{\{\Delta\phi\}_{\text{unpin}}}{2\pi} \times 100\%. \quad (3)$$

ρ_{uw} also means the success rate of an arbitrary $\Delta\phi$ whether or not can lead to successful unpinning under the given CPEF and excitability.

With given excitability which determines ω_s of an anchored spiral, ρ_{uw} is highly related to the angular frequency ω_e and strength E_0 of CPEF. Among a certain range of ω_e, ρ_{uw} can be optimized to its maximum. So we define the ω_e giving maximal ρ_{uw} as the optimal ω_e. Although different excitabilities (corresponding to different ω_s) have different optimal ω_e to optimize ρ_{uw}, the ratio of optimal ω_e over given ω_s keeps basically invariant. Thus we define this ratio as the optimal ω_e/ω_s. We illustrate this relation between ρ_{uw} and the optimal ω_e/ω_s, in the case of unpinning the counter-clockwise rotating anchored spiral in Barkley model under a certain excitability and electric strength, as red dotted line in Fig. 4. Beside optimal ω_e/ω_s, a proper electric strength E_0 can also optimize ρ_{uw}. As also shown in Fig. 4, larger E_0 makes larger ρ_{uw}. And there is a limit beyond which increasing E_0 makes no contribution to enhance ρ_{uw} any more. On the other hand, a high electric strength harms hearts. So this limit value (e. g. $E_0 = 1.8$ in Barkley model, as illustrated by black solid line in Fig. 4) could be used as the optimal electric strength.

Now with the optimal settings of CPEF (E_0, ω_e), we can examine the ability of CPEF to unpin anchored spirals in various excitabilities and compare it to the results by UEF. Firstly, to know how high the success rate (value of ρ_{uw}) is in various excitabilities, we take a part of

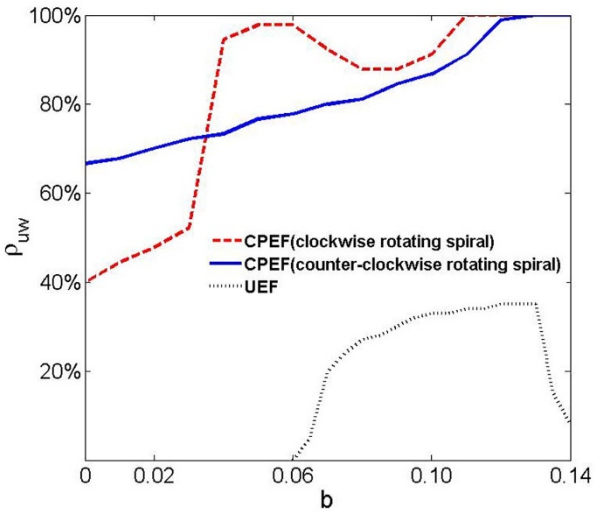

Figure 5 | A comparison of the success rate (value of ρ_{uw}) of CPEF and UEF in various excitabilities in Barkley model. The excitability is varied by changing b from 0 to 0.14 but fixing a to be 0.8. The blue solid and red dashed lines represent the success rate of unpinning counter-clockwise and clockwise spirals by CPEF respectively, at $E_0 = 1.8$, $\omega_e = 3.6\omega_s$. The black dotted line describes the success rate by UEF with the optimal strength $E_0 = 7$, which we get from simulations and is the same as in Fig. 5a of Ref. 31.

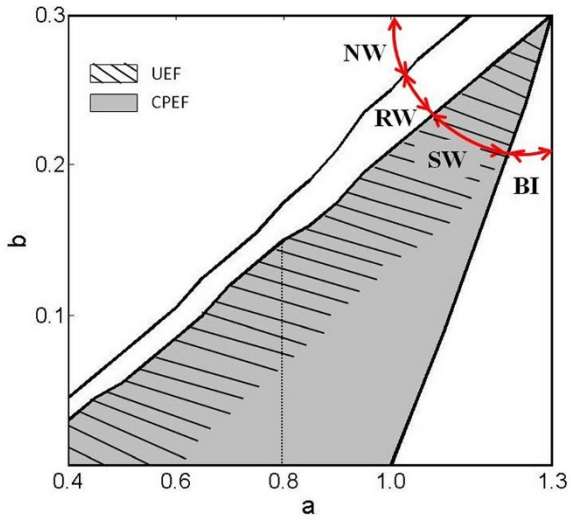

Figure 6 | A comparison of the application scope of CPEF and UEF in Barkley model. Three solid lines separate the whole parameter space about excitability into four regions marked by red double-headed arrows. In SW region, the medium exhibits excitable dynamics and supports spirals. For others, NW, RW and BI regions represent no wave, retracting waves and bi-stability, respectively. The shaded region represents successful unpinning by UEF with the optimal strength $E_0 = 7$, which we get from simulations and is the same as in Fig. 2b of Ref. 31. The gray region including the shaded region represents successful unpinning by CPEF ($E_0 = 1.8$, $\omega_e = 3.6\omega_s$). The vertical dotted line is corresponding to the chosen excitability used in Fig. 5.

excitability region ($a = 0.8$, $b = 0{\sim}0.14$) for instance, as Fig. 5 shows. In this excitability region, ρ_{uw} of CPEF reaches to an average of 80%, which is much higher than ρ_{uw} of UEF[31]. It is clear that CPEF is very effective in successfully unpinning both counter-clockwise (blue solid line) and clockwise (red dashed line) rotating anchored spirals. Especially in weak excitabilities ($b > 0.11$), ρ_{uw} of UEF is less than 40%, but ρ_{uw} of CPEF reaches 100%. This means that, regardless of $\Delta\phi$, CPEF can always successfully unpin anchored spirals in weak excitabilities. Moreover, in high excitabilities ($b<0.06$), UEF is failed at successfully unpinning any anchored spirals, but CPEF is still capable of successfully unpinning at an appreciable success rate ($\rho_{uw} > 40\%$). In addition, the optimal strength of CPEF ($E_0 = 1.8$) required for successful unpinning is much smaller than the optimal strength of UEF ($E_0 = 7$ in Ref. 31).

Beside of high success rate, in the parameter space about excitability, the application scope of CPEF, i.e. the extent where $\rho_{uw} > 0$, takes effect through the whole region where the medium exhibits excitable dynamics and supports spirals, and is much larger than the application scope of UEF[31]. This is illustrated in Fig. 6: The area representing the application scope of CPEF (gray region) fulfills the whole region where spirals sustain (SW region), but the area representing the application scope of UEF (shaded region) is just within a part of SW region. Since cardiac tissues may distribute across SW region, CPEF is more applicable than UEF to unpin anchored spirals.

In summary, we study the unique mechanism of WEH induced by CPEF, and find its outstanding ability to successfully unpin anchored spirals is better than UEF, at the higher success rate and larger application scope, even with a lower voltage. This is due to the unique characteristics of WEH induced by CPEF: in contrast to the dipole-like pattern induced by UEF[28,14–17], the pattern induced by CPEF is ancient-Taijitu-like (i.e. each of de-polarization and hyper-polarization has "Head" and "Tail") and rotates synchronously with the rotating CPEF. Therefore, in the case of unpinning by de-polarization, UEF would fail if the de-polarization is within the refractoriness of the anchored spiral and therefore cannot nucleate a new wave to unpin it. However, the rotating de-polarization induced by CPEF would escape from the refractoriness over time and nucleate a new wave easily. And the "Tail" of de-polarization induced by CPEF can form an unpinned new spiral's tip naturally, since it is originally unpinned. In the case of unpinning by hyper-polarization, UEF would fail if the hyper-polarization is not within the attached region of the anchored spiral and therefore cannot unpin it. However, the rotating hyper-polarization induced by CPEF would meet the attached region of the anchored spiral over time and unpin it easily. Moreover, the "Tail" of hyper-polarization induced by CPEF can drive the unpinned spiral further away from the obstacle, to prevent re-pinning which is an important cause to unsuccessful unpinning by UEF.

We believe, the outstanding ability of WEH induced by CPEF to unpin anchored spirals can be easily verified in cardiac tissues: instead of applying two DCs onto two pairs of field electrodes perpendicular to each other to deliver UEF in the experimental preparation of Fig. 5D in Ref. 16, one can apply two ACs onto these two pairs of field electrodes to realize CPEF in cardiac tissues, which is similar with the case in the Belousov-Zhabotinsky reaction of Ref. 35. We hope this lower-voltage higher-effectiveness approach may provide a better alternative to traditional therapies in terminating arrhythmia.

Methods

The Luo-Rudy model[36] can be expressed as

$$\frac{\partial V}{\partial t} = -\frac{I_{ion}}{C_m} + D\nabla^2 V$$
$$I_{ion} = I_{Na} + I_{si} + I_K + I_{K1} + I_{Kp} + I_b, \quad (4)$$

where V is the membrane potential, and I_{ion} is the total ionic currents which consist of a fast sodium current I_{Na}, a slow inward current I_{si}, a time-dependent potassium current I_K, a time-independent potassium current I_{K1}, a plateau potassium current I_{Kp}, and a time-independent background current I_b. $C_m = 1$ μF/cm² is the membrane capacitance, and D = 0.001 cm²/ms is the diffusion current coefficient.

In the polar coordinate, equation (4) is integrated on a $N_\rho \times M_\theta = 75 \times 336$ uniform grid with no-flux boundary conditions via Euler method, and a five-point finite difference scheme is applied to compute the Laplacian term $\nabla^2 V$. The space and time step are $\Delta\rho = 0.02$ cm, $\Delta\theta = \pi/168$ and $\Delta t = 0.001$ ms.

The Barkley model[37] can be expressed as

$$\frac{\partial u}{\partial t} = \varepsilon^{-1} u(1-u)\left(u - \frac{v+b}{a}\right) + \nabla^2 u$$
$$\frac{\partial v}{\partial t} = u - v, \quad (5)$$

where u is the fast variable corresponding to the membrane potential, and v is a slow variable corresponding to the recovery process. The parameter ε determines the timescale of u which is fixed to 0.02. And the parameters a and b control the excitability of the medium: Larger a increases the action potential duration and larger b/a increases the excitation threshold.

In the polar coordinate, equation (5) is integrated on a $N_\rho \times M_\theta = 91 \times 396$ uniform grid with no-flux boundary conditions via Euler method, and a five-point finite difference scheme is applied to compute the Laplacian term $\nabla^2 u$. The space and time step are $\Delta\rho = 1/6$, $\Delta\theta = \pi/198$ and $\Delta t = 2 \times 10^{-4}$.

1. Winfree, A. T. Spiral waves of chemical activity. *Science* **175**, 634–636 (1972).
2. Agladze, K. I. & Krinsky, V. I. Multi-armed vortices in an active-chemical medium. *Nature* **296**, 424–426 (1982).
3. Jakubith, S., Rotermund, H. H., Engel, W., von Oertzen, A. & Ertl, G. Spatiotemporal concentrtion patterns in a surface-reaction: propagating and standing waves, rotating spiral, and turbulence. *Phys. Rev. Lett.* **65**, 3013–3016 (1990).
4. Agladze, K., Keener, J. P., Müller, S. C. & Panfilov, A. Rotating spiral waves created by geometry. *Science* **264**, 1746–1748 (1994).
5. Vanag, V. K. & Epstein, I. R. Inwardly rotating spiral waves in a reaction-diffusion system. *Science* **294**, 835–837 (2001).
6. Sawai, S., Thomason, P. A. & Cox, E. C. An autoregulatory circuit for long-range self-organization in Dictyostelium cell populations. *Nature* **433**, 323–326 (2005).
7. Davidenko, J. M., Pertsov, A. V., Salomonsz, R., Baxter, W. & Jalife, J. Stationary and drifting spiral waves of excitation in isolated cardiac-muscle. *Nature* **355**, 349–351 (1992).
8. Gray, R. A., Pertsov, A. M. & Jalife, J. Spatial and temporal organization during cardiac fibrillation. *Nature* **392**, 75–78 (1998).
9. Witkowski, F. X. *et al*. Spatiotemporal evolution of ventricular fibrillation. *Nature* **392**, 78–82 (1998).
10. Biktashev, V. N., Holden, A. V. & Zhang, H. Tension of organizing filaments of scroll waves. *Phil. Trans. R. Soc.Lond. A* **347**, 611–630 (1994).
11. Alonso, S., Sagués, F. & Mikhailov, A. S. Taming Winfree turbulence of scroll waves in excitable media. *Science* **299**, 1722–1725 (2003).
12. Zhang, H., Cao, Z. J., Wu, N. J., Ying, H. P. & Hu, G. Suppress Winfree turbulence by local forcing excitable systems. *Phys. Rev. Lett.* **94**,188301 (2005).
13. Gray, R. A. & Wikswo, J. P. Several small shocks beat one big one. *Nature* **475**, 181–182 (2011).
14. Ripplinger, C. M., Krinsky, V. I., Nikolski, V. P. & Efimov, I. R. Mechanisms of unpinning and termination of ventricular tachycardia. *Am. J. Physiol. Heart Circ. Physiol.* **291**, H184–H192 (2006).
15. Cysyk, J. & Tung, L. Electric field perturbations of spiral waves attached to millimeter-size obstacles. *Biophys. J.* **94**, 1533–1541 (2008).
16. Fenton, F. H. *et al*. Termination of atrial fibrillation using pulsed low-energy far-field stimulation. *Circulation* **120**, 467–464 (2009).
17. Luther, S. *et al*. Low-energy control of electrical turbulence in the heart. *Nature* **475**, 235–239 (2011).
18. Weidmann, S. Effect of current flow on the membrane potential of cardiac muscle. *J. Physiol.* **115**, 227–236 (1951).
19. Sepulveda, N. G., Roth, B. J. & Wikswo Jr, J. P. Current injection into a two-dimensional anisotropic bidomain. *Biophys. J.* **55**, 987–999 (1989).
20. Sobie, E. A., Susil, R. C. & Tung, L. A generalized activating function for predicting virtual electrodes in cardiac tissue. *Biophys. J.* **73**, 1410–1423 (1997).
21. Fishler, M. G. Syncytial heterogeneity as a mechanism underlying cardiac far-field stimulation during defibrillation-level shocks. *J. Cardiovasc. Electr.* **9**, 384–394 (1998).
22. Fast, V. G., Rohr, S., Gillis, A. M. & Kléber, A. G. Activation of cardiac tissue by extracellular electrical shocks: Formation of 'Secondary sources' at intercellular clefts in monolayers of cultured myocytes. *Circ. Res.* **82**, 375–385 (1998).
23. Trayanova, N. & Skouibine, K. Modeling defibrillation - Effects of fiber curvature. *J. Electrocardiol.* **31**, 23–29 (1998).
24. Hooks, D. A. *et al*. Cardiac microstructure: Implications for electrical propagation and defibrillation in the heart. *Circ. Res.* **91**, 331–338 (2002).
25. Woods, M. C. *et al*. Virtual electrode effects around an artificial heterogeneity during field stimulation of cardiac tissue. *Heart Rhythm* **3**, 751–752 (2006).
26. Pumir, A. & Krinsky, V. Unpinning of a rotating wave in cardiac muscle by an electric field. *J. Theor. Biol.* **199**, 311–319 (1999).
27. Takagi, S. *et al*. A physical approach to remove anatomical reentries: a bidomain study. *J. Theor. Biol.* **230**, 489–497 (2004).
28. Takagi, S. *et al*. Unpinning and removal of a rotating wave in cardiac muscle. *Phys. Rev. Lett.* **93**, 058101 (2004).
29. Pumir, A. *et al*. Wave emission from heterogeneities opens a way to controlling chaos in the heart. *Phys. Rev. Lett.* **99**, 208101 (2007).
30. Bittihn, P. *et al*. Far field pacing supersedes anti-tachycardia pacing in a generic model of excitable media. *New J. Phys.* **10**, 103012 (2008).
31. Bittihn, P. *et al*. Phase-resolved analysis of the susceptibility of pinned spiral waves to far-field pacing in a two-dimensional model of excitable media. *Phil. Trans. R. Soc. A* **368**, 2221–2236 (2010).
32. Bittihn, P., Hörning, M. & Luther, S. Negative curvature boundaries as wave emitting sites for the control of biological excitable media. *Phys. Rev. Lett.* **109**, 118106 (2012).
33. Cai, M. C., Pan, J. T. & Zhang, H. Electric-field-sustained spiral waves in subexcitable media. *Phys. Rev. E* **86**, 016208 (2012).
34. Li, B. W., Deng, L. Y. & Zhang, H. Chiral symmetry breaking in a reaction-diffusion system. *Phys. Rev. E* **87**, 042905 (2013).
35. Ji, L., Zhou, Y., Li, Q., Qiao, C. & Ouyang, Q. Experimental evidence of using a circularly polarized electric field to control spiral turbulence. *Phys. Rev. E* **88**, 042919 (2013).
36. Luo, C. H. & Rudy, Y. A model of the ventricular cardiac action potential. depolarization, repolarization, and their interaction. *Circ. Res.* **68**, 1501–1526 (1991).
37. Barkley, D. A model for fast computer simulation of waves in excitable media. *Physica D* **49**, 61–70 (1991).
38. Xie, F. G., Qu, Z. L., Garfinkel, A. & Weiss, J. N. Electrophysiological heterogeneity and stability of reentry in simulated cardiac tissue. *Am. J. Physiol. Heart Circ. Physiol.* **280**, H535–H545 (2001).

Acknowledgments

This work was supported by the National Natural Science Foundation of China under Grants No. 11275167, No. 10975117, No. 11205039, and the Program for New Century Excellent Talents in University.

Author contributions

H.Z. and B.-W.L. conceived the concept of using CPEF to unpin spiral waves. X.F., X.G. and D.-B.P. developed this approach and performed numerical simulations and data analysis. X.G., X.F. and H.Z. contributed to the discussions about unpinning mechanisms by CPEF. X.F., X.G. and H.Z. wrote the manuscript with input from all authors.

Additional information

Competing financial interests: The authors declare no competing financial interests.

How to cite this article: Feng, X., Gao, X., Pan, D.-B., Li, B.-W. & Zhang, H. Unpinning of rotating spiral waves in cardiac tissues by circularly polarized electric fields. *Sci. Rep.* **4**, 4831; DOI:10.1038/srep04831 (2014).